Advances in Science and Technology Research Journal

Advances in Science and Technology Research Journal, 2025, 19(10), 136–149
https://doi.org/10.12913/22998624/208238
ISSN 2299-8624, License CC-BY 4.0

Received: 2025.06.18
Accepted: 2025.08.15
Published: 2025.09.01

Modeling and analysis of fiber laser cutting conditions on the surface quality of stainless steel 201

Anwar Hassan Zabon[1], Tahseen Fadhil Abbas[2], Aqeel Sabree Bedan[1*]

[1] Department of Production Engineering and Metallurgy, University of Technology, 52 street, Baghdad, Iraq
[2] Department of Aeronautical Technical Engineering, College of Technical Engineering, Al-Farahidi University, Iraq
* Corresponding author's e-mail: Aqeel.S.Bedan@uotechnology.edu.iq

ABSTRACT

Austenitic stainless steel grade 201 is widely used in industrial applications due to its corrosion resistance and cost-effectiveness. However, Laser cutting is known for its speed, precision, and cost-effectiveness, but still has some limitations in achieving high surface quality, particularly when oxygen is used as the assist gas. This study investigates and optimizes the fiber laser cutting (FLC) process for SS201 using a central composite design (CCD) under response surface methodology (RSM). Five machining parameters were examined: laser power (Pu), cutting speed (v), assist gas pressure (P), pulse frequency (F), and focal point position (FP), with their effects evaluated on three key quality characteristics: top kerf width (TKW), bottom kerf width (BKW), and kerf taper (KT). Analysis of variance (ANOVA) revealed that laser power had the most significant influence on BKW (72%) and TKW (61%), while gas pressure had the strongest effect on KT (40.6%). The optimal results were achieved under different parameter settings for each quality measure: the minimum TKW of 369.64 µm, the lowest BKW of 507.12 µm, and the minimum KT of 0.011°. These findings highlight the necessity of multi-objective optimization and the importance of parameter-specific control strategies to enhance cut quality in laser processing of stainless steel.

Keywords: fiber laser, kerf taper, top kerf width, bottom kerf width, response surface methodology.

INTRODUCTION

Stainless steel has played a vital role in industrial, structural, and medical applications for decades, largely due to its durability and resistance to corrosion [1, 2]. However, machining it using traditional methods poses challenges such as tool wear, poor finish, and high cost [3]. Fiber laser cutting (FLC) is increasingly adopted for its precision, minimal distortion, and efficiency [4, 5]. Technological advances in high-power laser systems and CNC integration have further improved quality and flexibility [6, 7]. Nonetheless, the performance of laser cutting is highly dependent on the specific material properties and equipment used. Therefore, parameter optimization is essential to ensure the high cut quality and maintain the surface integrity in stainless steel processing [8]. Pramanik and et al. Assessed experimentally the impact of the laser's parameters v, F, and Pu on the Ra and KT on FLC of 1 mm Ti-6Al-4V sheets. The findings were highlighted in order to get the predicted min. KT of 0.4244°, min. Ra of 2.2946 µm, 46.9884 W of power, 52.9097 kHz pulse frequency, and 0.5634 mm/sec speed [9]. Genna et al. investigated CO_2 laser cutting of AISI 304, AlMg3, and St37-2 plates, focusing on how v, P, T, FP, ND, and gas type (TOG) affect Ra, KW, and KT. Using ANOVA and FFD, they found that v, FP, had the most impact on the Ra and KW. [10]. Patel et al. used RSM to examine the CO_2 laser cutting of EN-31 die steel plates that had 10 mm thick. Analysis was done on how Pu, v, P, and F affected KT, Ra, and heat affected zone (HAZ). The findings showed that the higher v and lower F reduced KT and Ra [11]. Rajamani et al. mentioned that utilizing the Hastelloy C276 laser cutting with Nd:YAG sheets that were 3 mm thick was examined. They looked

at how Pu, v, P and SOD affected KT and Ra. they found that KT is minimized by using high v and moderate Pu. While the high standoff distance raised the surface roughness and kerf taper [12]. Alsaadawy et al. employed the cutting parameters, such as the v, and P; Ra, kerf width, kerf taper, and slag height Sh were the characteristics that significantly affected the cutting quality. The fundamental factors affecting the minimum slit width and minimum slit taper values were determined [13]. Li et al. examined the high-power FLC of CFRP laminates that were 10 mm thick. Using a single-pass approach, analysis was done on how Pu, v affected KW, and KT. According to the results, KW was decreased, when high v and moderate Pu were coupled. Wider kerfs, delamination, and thermal flaws were induced by low v or excessive Pu [14]. Y. Singh et al. examined the pulsed CO_2 laser cutting of hybrid composites with thicknesses ranging from 3 to 4.5 mm. RSM was used to examine how v, P, FP, and PW affected KT and Ra. The outcomes demonstrated that the optimized PW and FP reduced KT and greatly enhanced surface quality. KT rose as the P and F increased [4]. Nguyen et al. examined the FLC of sheets of SS-304 stainless steel that were 3 mm thick. The impacts of Pu, v, P, and FP on the top kerf width (TKW), bottom kerf width (BKW), and Ra. they found that reducing the Ra and Careful control of v was necessary to ensure precise cutting profiles [15]. Based on the research reviewed in earlier studies, the impact of Pu, v, F, T, P FP, nozzle diameter (ND), type of gas (TOG) and stand-off distance (SOD), Prior studies mostly addressed thinner sheets, other steel grades, or used nitrogen, often analyzing parameters individually, which limited holistic optimization. creating a gap in research that needs to be filled. Thus, parameters – Pu, v, P, F, and FP – on TKW, BKW, and KT in SS201 using oxygen as the assist gas. A central composite design (CCD) based on response surface methodology (RSM) was used to analyze and optimize cutting performance.

EXPERIMENTAL PROCEDURES

The experimental procedures were conducted using a high-power Fiber laser cutting FLC system (IGR-3015F, IGOLDEN CNC), capable of delivering up to 12,000 watts of output power. The machine supports a maximum cutting area of 3000 × 1500 mm, making it suitable for processing large metal sheets. All experimental programming was carried out using standard CNC techniques, and the scanner and air nozzle were mounted on a typical 3-axis CNC machine. Nozzle circular Shape Single type with diameter 3 mm, The oxygen gas was selected. The LC machine and the general parts of its auxiliary supply are shown in Figure 1.

The workpiece (W.P) material was austenitic stainless steel grade 201, a low-nickel alloy that contains elevated levels of manganese and chromium. Table 1 presents the chemical composition of the selected material, as per ASM standards.

Experimental tests were carried out on SS201 plates (40 mm wide, 5 mm thick), consisting of two pieces measuring 500 mm and one piece 750 mm in length. A comb-cut layout was used to ensure thermal isolation between cuts, maintaining 50 mm spacing and a cutting length of 35 mm. Following LC, the plates were divided into 32 identical specimens (50 × 40 × 5 mm) with the groove centrally positioned for

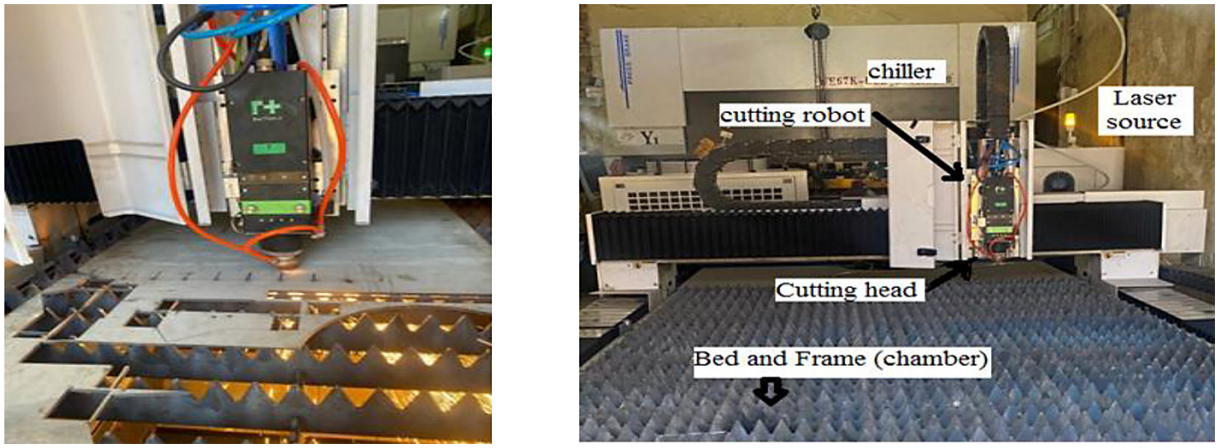

Figure 1. The general view of the laser cutting machine

Table 1. Chemical composition (wt.%) and the ASM standard for Stainless Steel 201

Element	C%	Si%	Mn%	P%	Cr%	Mo%	Ni%	Cu%
Weight %	0.136	0.219	5	< 0.0005	16	< 0.002	4.09	0.284
ASM	0.15	1	5.5–7.5	0.060	16–18	-	3.5–5.5	-

uniform quality evaluation. Final separation was performed using waterjet cutting to eliminate any thermal or mechanical deformation, as illustrated in Figure 2.

To systematically assess the impact of multiple input parameters and their interactions on the output responses, RSM was applied [16] [17]. A CCD was chosen to build the experimental matrix, providing a structured approach to evaluate the influence of five independent process parameters, each varied at three levels: These parameters include:

- Laser power (Pu) [2000, 6000, 10000 W]
- Cutting speed (v) [0.5, 1.0, 1.5 mm/min]
- Assist gas pressure (P) [7, 10, 13 bar]
- Pulse frequency (F) [100, 2550, 5000 Hz]
- Focal point position (FP) [-25, -12, +1 mm]

The experimental design comprised 32 runs, including 6 center points to improve the accuracy and robustness of the regression model. This range was selected based on machine capability and preliminary experiments to ensure beam convergence across material thickness.

MEASUREMENT OF CUTTING QUALITY

Measurement of the kerf width (KW)

The two main quality indicators, top kerf width (TKW) and bottom kerf width (BKW), were assessed along the workpiece (WP) with a (35 mm) linear cutting path. Kerf width can be calculated on the basis of difference in the dimension of cutting edge. The workpiece materials were kept horizontal during the entire experiment and were used to measure the widths, using metallurgical incident light Microscope KRUSS – model Mbl3300 microscope (4X), as displayed showing in Figure 3

Three different points (K1, K2, and K3) were selected for measuring the TKW and 3 in bottom kerf width, as shown in Figure 4 (a–b).

Measurement of the kerf taper (KT)

Using the measured values of TKW and BKW, the kerf taper (KT) was computed for each specimen using Equation bellow:

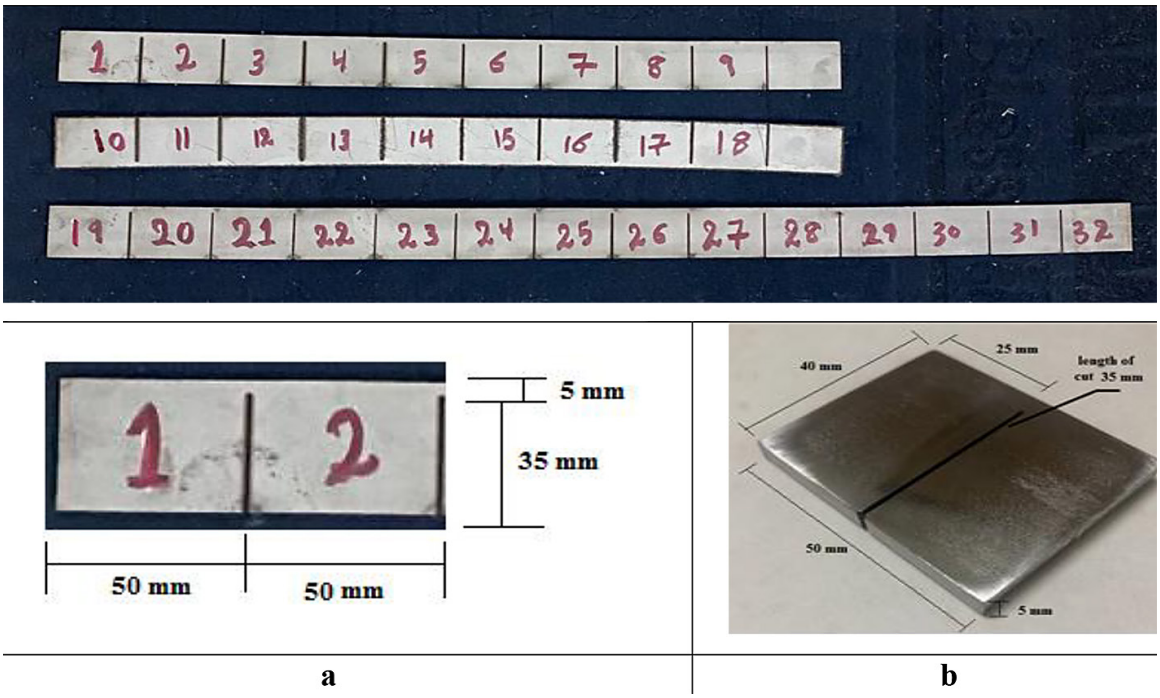

Figure 2. Samples (a) with central notch created by Fiber LC, (b) with Created by WJM, with dimensions

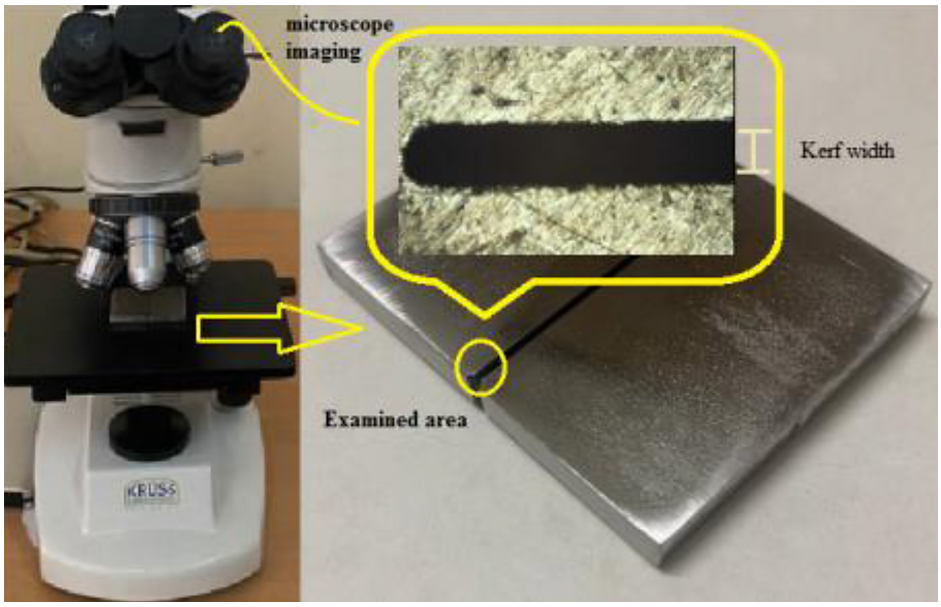

Figure 3. General view of the light microscope

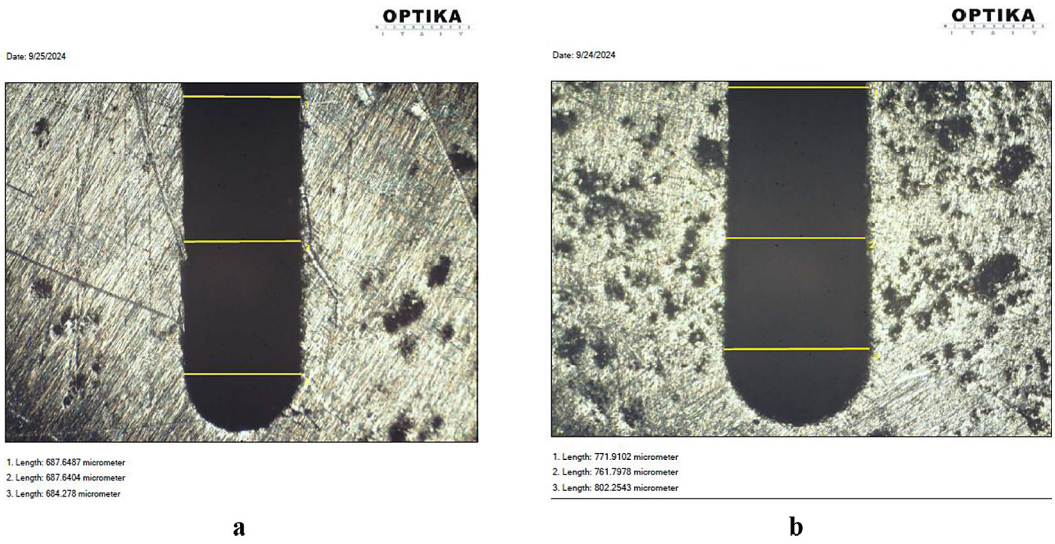

Figure 4. Microscopic image of the cut with measurement points (a) Top kerf width (b), Bottom kerf width

$$KT = tan\text{-}1\left(\frac{TKW - BKW}{2 \times t}\right) \qquad (1)$$

Figure 5 show the Schematic diagram showing the kerf taper angle (KT).

While both surface roughness (Ra) and HAZ are commonly assessed in laser cutting research, they were excluded from this study. The main focus was placed on kerf geometry characteristics (TKW, BKW, KT), which are critical for dimensional precision and taper control. Ra measurement requires high-resolution surface metrology equipment, and HAZ analysis involves metallographic inspection tools that were not available during the experimental phase. Future work will incorporate these quality indicators to provide a more comprehensive evaluation of laser cutting performance. The measured values of TKW and BKW are listed in Table 2.

RESULT AND DISCUSSION

The results and discussion are structured into four main sections: analysis of top kerf width, analysis of bottom kerf width, kerf taper (KT) analysis, and interaction effects and physical interpretation

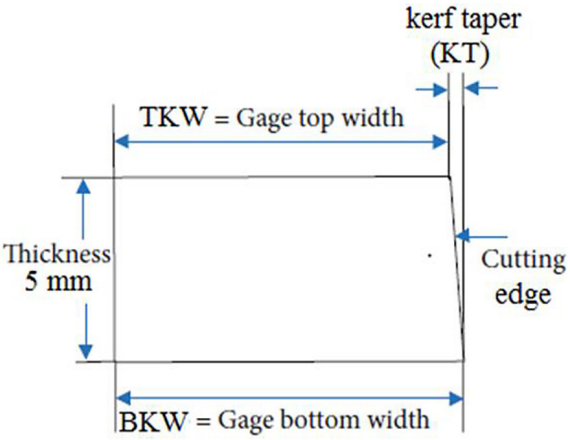

Figure 5. Schematic diagram of kerf taper [13]

Analysis of top kerf width

In order to better comprehend how laser cutting settings affect TKW, the analysis is divided into four sections: This structure allows for both statistical rigor and practical insight into the behavior of the response variable under varying process conditions.

ANOVA results

ANOVA was used to assess the significance of input variables. Table 3 lists F- and p-values, where $p < 0.05$ indicates statistical significance at 95% confidence [18] [19]. TKW was significantly

Table 2. Experimental values of SR and DA in micrometer based on RSM technique

Run #	(Pu) watt	(V) mm/min	(P) bar	(F) Hz	(FP) mm	(TKW) µm	(BKW) µm	(KT) °
1	10000	1.5	7	100	1	531.1	1168.5	3.647
2	2000	0.5	7	100	1	990.5	992.5	0.011
3	2000	1.5	13	100	1	629.2	1197.4	3.251
4	6000	1.0	10	2550	1	912.1	1149.8	1.361
5	6000	1.0	7	2550	-12	765.5	959.6	1.111
6	6000	1.0	10	2550	-12	1042.7	1131.5	0.508
7	2000	1.5	13	5000	-25	694.8	1053.7	2.055
8	10000	1.0	10	2550	-12	634.1	990.8	2.043
9	10000	1.5	13	5000	1	658.8	735.0	0.436
10	6000	1.0	10	5000	-12	484.7	546.9	0.356
11	6000	1.0	10	2550	-12	487.4	979.2	2.815
12	2000	0.5	13	5000	1	503.3	635.8	0.758
13	6000	0.5	10	2550	-12	425.1	928.3	2.880
14	2000	0.5	7	5000	-25	464.8	605.7	0.807
15	6000	1.0	13	2550	-12	369.6	843.3	2.711
16	6000	1.0	10	2550	-12	494.0	648.7	0.886
17	2000	0.5	13	100	-25	401.1	618.9	1.247
18	6000	1.0	10	2550	-12	482.0	914.9	2.478
19	10000	0.5	7	100	-25	556.2	694.0	0.789
20	10000	1.5	13	100	-25	493.6	694.5	1.150
21	2000	1.0	10	2550	-12	681.3	966.2	1.632
22	2000	1.5	7	100	-25	456.6	507.1	0.290
23	2000	1.5	7	5000	1	597.0	652.2	0.317
24	10000	0.5	13	100	1	620.2	643.2	0.132
25	6000	1.0	10	2550	-25	786.4	788.9	0.014
26	10000	1.5	7	5000	-25	578. 5	612.9	0.198
27	10000	0.5	7	5000	1	609.2	657.9	0.279
28	6000	1.0	10	2550	-12	599.7	661.3	0.353
29	10000	0.5	13	5000	-25	614.6	656.7	0.241
30	6000	1.5	10	2550	-12	617.9	649.4	0.179
31	6000	1.0	10	100	-12	595.0	688.2	0.534
32	6000	1.0	10	2550	-12	589.3	694.0	0.599

influenced by all machining parameters (A–E). The R^2 and Adjusted R^2 differed by less than 20%, confirming model adequacy [20].

Regression equation in uncoded units.

$$\begin{aligned} \text{TKW} &= 1416 - 0.1602\,\text{A} - 283\,\text{B} + \\ &+ 28.8\,\text{C} + 0.1206\,\text{D} + 25.56\text{E} + \\ &+ 0.00007\text{A} \times \text{A} + 123.9\text{B} \times \text{B} - \\ &- 1.72\,\text{C} \times \text{C} - 0.000017\,\text{D} \times \text{D} + \\ &+ 1.268\,\text{E} \times \text{E} + 0.01665\,\text{A} \times \text{B} + \\ &+ 0.002946\,\text{A} \times \text{C} + 0.000978\,\text{A} \times \text{E} - \\ &- 0.02162\,\text{B} \times \text{D} - 2.69\text{B} \times \text{E} - +0.802\,\text{C} \times \text{E} \end{aligned} \quad (2)$$

Contribution percentages

As shown in Figure 6 ANOVA results showed that all five machining parameters significantly affected TKW. Pu had the highest impact (61%), followed by FP (28%), P (4.5%), v (3.8%), and F (2.7%). Figure 7 illustrates the percentage contribution of each factor.

Residual plot analysis

Figure 7 presents the four-in-one residual plots used to validate ANOVA assumptions and regression adequacy [4]. The residuals show normal distribution, homoscedasticity, and independence – confirmed by the normal probability plot, residuals vs. fitted values, residuals vs. observation order, and histogram. These results confirm the model's validity and its reliability for predicting TKW.

Main effects plot analysis

Main effects plots (Figure 8) were used to analyze the impact of machining parameters on TKW. Increasing Pu noticeably reduced TKW due to higher energy density enhancing melting and vaporization. While cutting speed (v) and frequency (F) had smaller contributions, their effects were still statistically significant.

Analysis of bottom kerf width

To gain a deeper understanding of the impact of LC parameters on BKW, the analysis is structured into four parts:

ANOVA results

ANOVA results for BKW (Table 4) show that all five machining parameters significantly affect BKW ($p < 0.05$). Laser power (A) and focal position (E) had the strongest effects, with F-values of 1419.87 and 337.41. Cutting speed (B), gas pressure (C), and frequency (D) were also significant. The model showed excellent fit with R^2 = 99.58%, adjusted R^2 = 98.81%, and predicted R^2 = 70.22%, confirming its predictive reliability.

Regression equation in uncoded units

$$\begin{aligned} BKW(\mu m) &= 490 - 0.06141A + \\ &+ 868.7B - 18.2\,C + 0.0911\,D + \\ &+ 0.28E\;0.000001\,A \times A - 294.4\,B \times \\ &\times B + 1.12\,C \times C - 0.000013\,D \times D + \\ &+ 0.8008E \times E - + 0.002544\,A \times C + \\ &+ 0.000001\,A \times D + 0.001197\,A \times E - \\ &- 20.33\,B \times C - - 0.01383\,B \times D + \\ &+ 3.863\,B \times E - 0.002872\,C \times D + \\ &+ 0.000710\,D \times E \end{aligned} \quad (3)$$

Table 3. ANOVA for TKW

Source	DF	Adj SS	Adj MS	F Value	P Value	VIF
Liner	5	640837	63140	59.18	0.000	
A: laser power	1	392246	392246	367.67	0.000	1.00
B: cutting speed	1	24293	24293	22.77	0.001	1.00
C: gas pressure	1	28493	28493	26.71	0.000	1.00
D: frequency	1	16939	16939	15.88	0.002	1.00
E: focal position	1	178865	178865	167.66	0.000	1.00
2-way interaction	10	122539	12254	11.49	0.000	
A*B	1	17748	17748	16.64	0.002	1.00
A*C	1	19995	19995	18.74	0.001	1.00
A*E	1	41391	41391	38.80	0.000	1.00
B*D	1	11218	11218	10.51	0.008	1.00
B*E	1	4897	4897	4.59	0.055	1.00
C*E	1	15657	15657	14.68	0.003	1.00

Note: Model summary: S = 32.6628, R – sq = 99.08%, R – sq(adj) = 97.41%, R – sq(pred) = 21.90%.

Contribution percentages

The ANOVA results for BKW indicated that all five machining parameters had a significant influence on BKW. Laser power was the most dominant factor, contributing for 72% of the variation in BKW, followed by focal position at 17%, frequency at 8%, gas pressure at 2%, and cutting speed at 1%. A pie chart illustrating the proportional contribution of machining factors to BKW is displayed in Figure 9.

Residual plot analysis

Figure 10 presents the residual plots for BKW, used to validate regression assumptions of normality, independence, and constant variance. The normal probability plot shows a straight-line pattern, indicating normal distribution. Residuals vs. fitted values exhibit random scatter, confirming homoscedasticity. No trends appear in the observation order plot, and the histogram is bell-shaped. These results confirm the model's validity and predictive reliability.

Main effects plot analysis

Main effects plots (Figure 11) illustrate how machining parameters affect BKW. Laser power had the strongest influence, with higher levels improving melting and ejection, resulting in narrower kerfs. Focal position also showed a major effect, with –12 mm minimizing BKW. Frequency had a non-linear effect, with optimal performance around 2000 Hz. While gas pressure and cutting speed had smaller impacts, both were statistically significant: higher pressure improved ejection, and cutting speed showed a U-shaped trend with minimal BKW at both extremes.

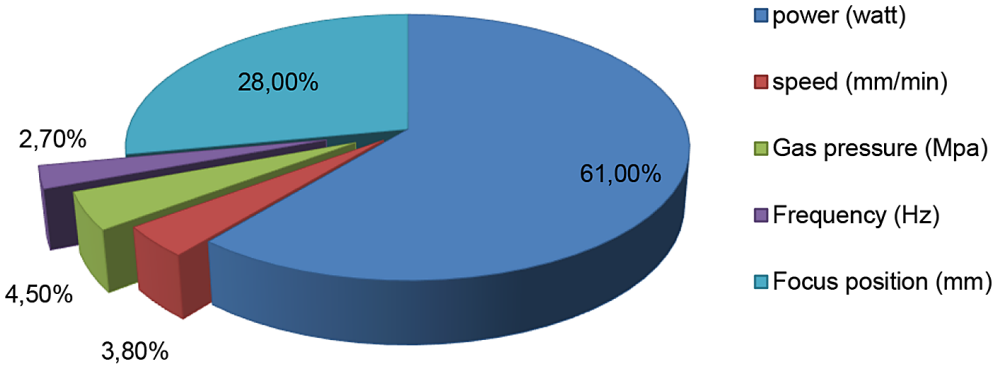

Figure 6. Percentage contribution of machining parameters to TKW

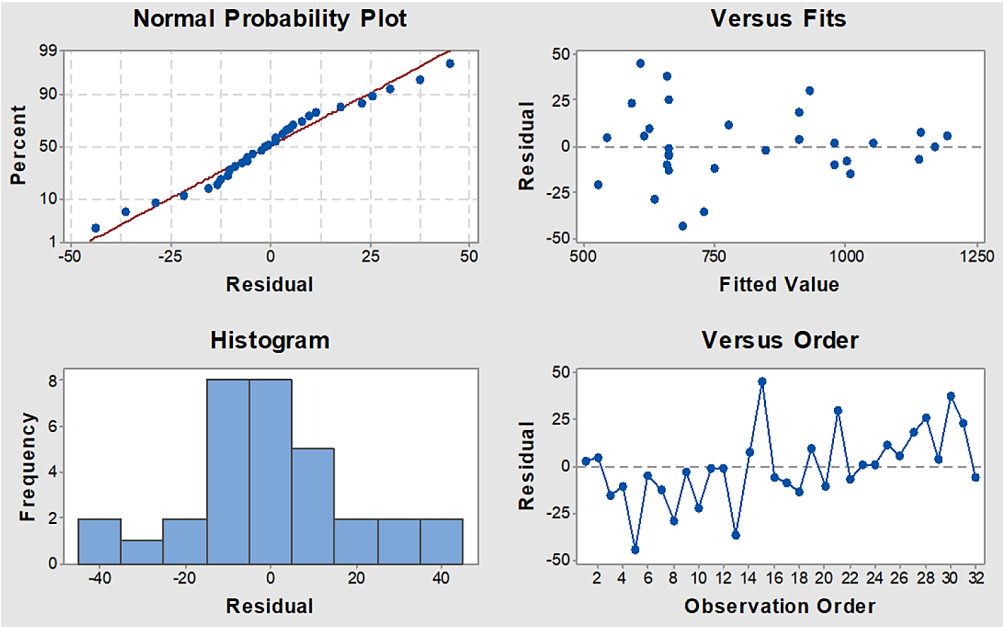

Figure 7. Four-in-one residual plots for TKW

Table 4. ANOVA for BKW

Source	DF	Adj SS	Adj MS	F-Value	P-Value	VIF
Liner	5	579951	115990	392.89	0.000	
A: laser power	1	419180	419180	1419.87	0.000	1.00
B: cutting speed	1	3440	3440	11.65	0.006	1.00
C: gas pressure	1	11932	11932	40.42	0.000	1.00
D: frequency	1	45787	45787	155.09	0.000	1.00
E: focal position	1	99611	99611	337.41	0.000	1.00
2-way interaction	10	125581	12558	42.54	0.000	
A*C	1	14916	14916	50.53	0.000	1.00
A*D	1	2845	2845	9.64	0.010	1.00
A*E	1	62007	62007	210.03	0.000	1.00
B*C	1	14877	14877	50.39	0.000	1.00
B*D	1	4591	4591	15.55	0.002	1.00
B*E	1	10090	10090	34.18	0.000	1.00
C*D	1	7128	7128	24.14	0.000	1.00
D*E	1	8178	8178	27.70	0.000	1.00

Note: Model Summary: S = 17.1821, R – sq = 99.58%, R – sq(adj) = 98.81%, R – sq(pred) = 70.22%.

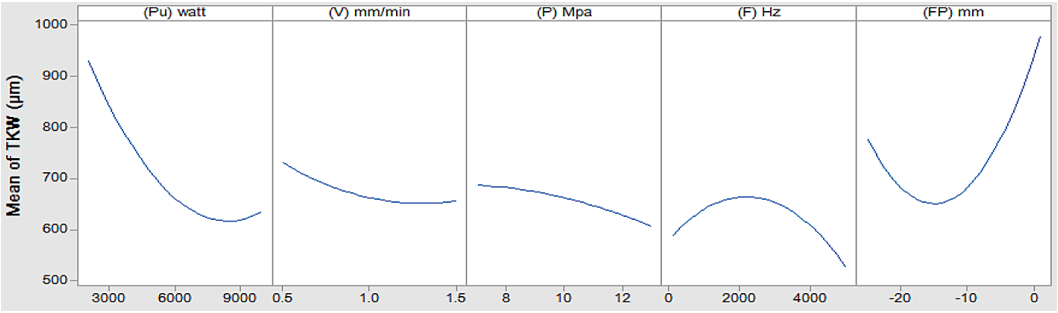

Figure 8. Main effects plot influence of machining parameters on the TKW

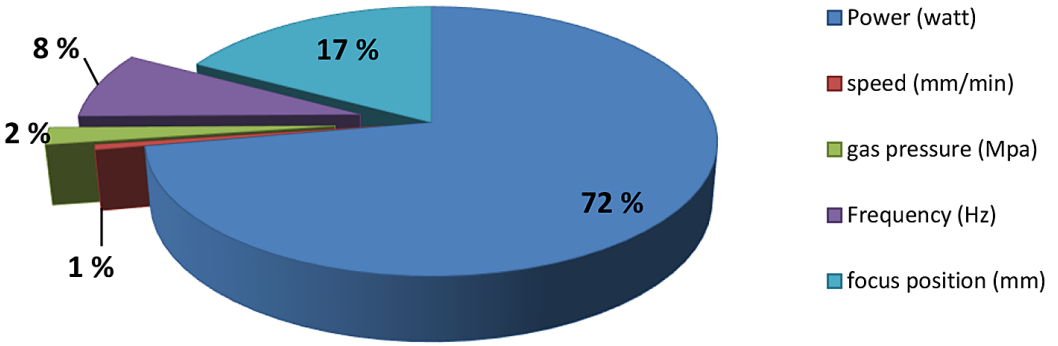

Figure 9. Percentage contribution of machining parameters to BKW

Kerf taper (KT) analysis

Kerf taper (KT) values were calculated based on the top and bottom kerf widths, The following analysis examines the variation of KT across the 32 experimental runs and its correlation with the input process parameters.

ANOVA results

To assess the impact of the five machining parameters, a full quadratic regression model was applied. The ANOVA results are summarized in Table 5. The analysis revealed that none of the main input parameters had statistically significant

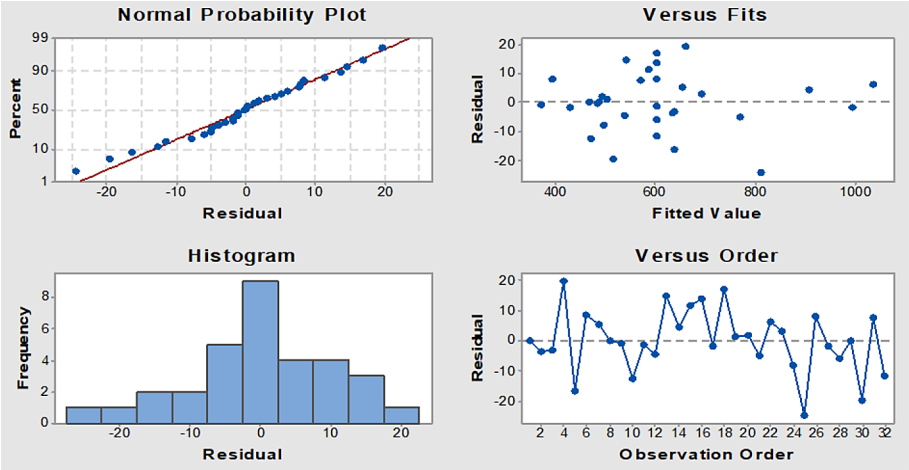

Figure 10. Four-in-one residual plots for bottom kerf width (BKW)

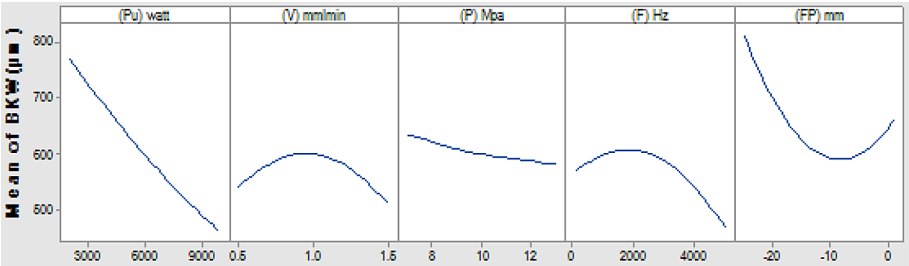

Figure 11. Main effects plot influence of machining parameters on the (BKW)

effects on KT at a 95% confidence level, as all p-values for the main effects were greater than 0.05 [21]. The only interaction term that approached statistical relevance was A*C ($p = 0.061$), but it still exceeded the standard significance threshold. The model's R-squared value was 62.40%, indicating a moderate ability to explain the variation in the observed data. Although the regression model explained 62.4% of the variance in the observed KT values, both the adjusted R^2 and predicted R^2 values were 0.00%, clearly indicating overfitting and a lack of generalizability. This means that the current model cannot be relied upon to predict KT for new parameter combinations and should be used for descriptive analysis only.

To overcome this limitation, future studies should consider increasing the number of experimental runs and exploring nonlinear modeling techniques or machine learning methods (e.g., artificial neural networks or regression trees) to improve the predictive performance of KT modeling.

Contribution percentages

ANOVA results (Table 5) show that gas pressure is the most significant factor affecting KT, contributing 40.6%, followed by frequency (26%) and cutting speed (23%). This marks a notable shift from earlier assumptions, highlighting the strong influence of thermal and gas-related parameters (P and F) on KT. Accurate control of these variables is essential to ensure consistent cut geometry. Figure 12 presents the percentage contributions in a pie chart.

Residual plot analysis

Figure 13 presents the four-in-one residual plots for KT, used to validate ANOVA assumptions of normality, independence, and homoscedasticity [20]. The normal probability plot shows an approximately straight line, indicating normal distribution. Residuals vs. fitted values and observation order plots show random scatter, confirming constant variance and independence. The bell-shaped histogram further supports normality, validating the KT regression model.

Main effects plot analysis

The main effects plot for KT (Figure 14) shows that P had the greatest impact, forming a U-shaped

Table 5. ANOVA for KT

Source	DF	Adj SS	Adj MS	F Value	P Value	VIF
Liner	5	0.87288	0.17458	0.66	0.664	
A: laser power	1	0.03723	0.03723	0.14	0.716	1.00
B: cutting speed	1	0.20154	0.20154	0.76	0.403	1.00
C: gas pressure	1	0.35470	0.35470	1.33	0.273	1.00
D: frequency	1	0.22608	0.22608	0.85	0.377	1.00
E: focal position	1	0.05334	0.05334	0.20	0.663	1.00
2-way interaction	10	2.76263	0.27626	1.04	0.473	
A*B	1	0.01396	0.01396	0.05	0.823	1.00
A*C	1	1.16272	1.16272	4.37	0.061	1.00
A*D	1	0.33526	0.33526	1.26	0.286	1.00
A*E	1	0.09254	0.09254	0.35	0.567	1.00
B*C	1	0.07419	0.07419	0.28	0.608	1.00
B*D	1	0.40199	0.40199	1.51	0.245	1.00
B*E	1	0.55658	0.55658	2.09	0.176	1.00
C*D	1	0.00065	0.00065	0.00	0.961	1.00
C*E	1	0.03496	0.03496	0.13	0.724	1.00
D*E	1	0.08978	0.08978	0.34	0.573	1.00

Note: Interaction terms (A*C*, *B*E, etc.) also showed no statistical significance, with all p-values exceeding 0.05. Model summary: S = 0.516062, R-sq. = 62.40%, R-sq(adj) = 0.00%, R-sq(pred) = 0.00%.

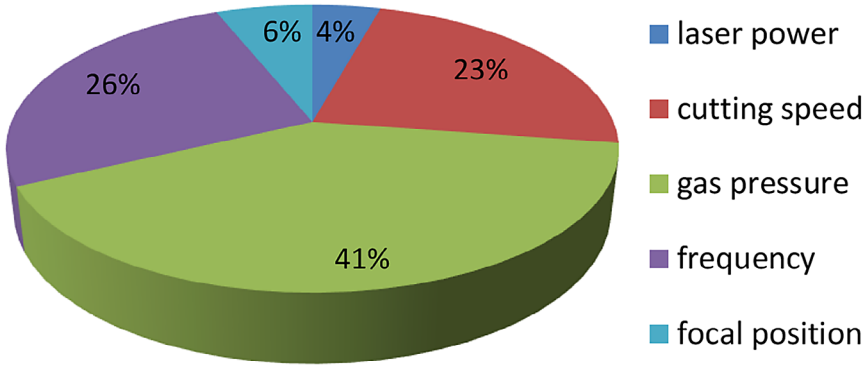

Figure 12. Percentage contribution of machining parameters to KT

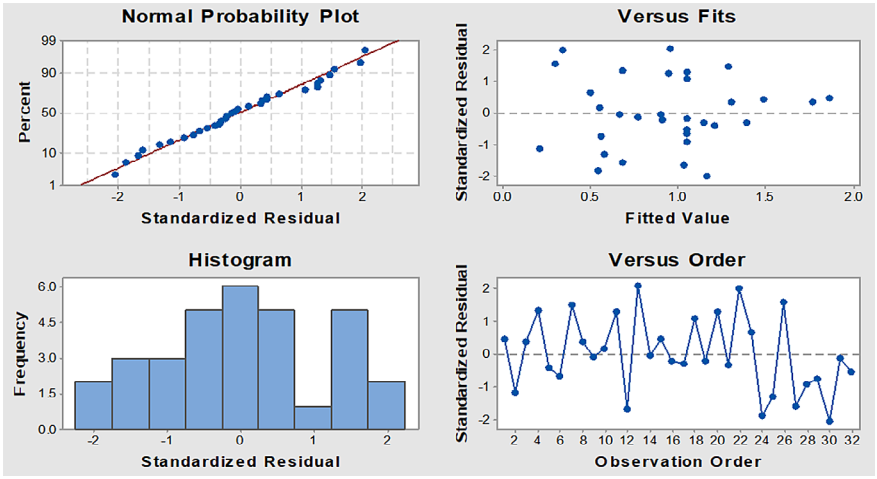

Figure 13. Four-in-one residual plots for kerf taper (KT)

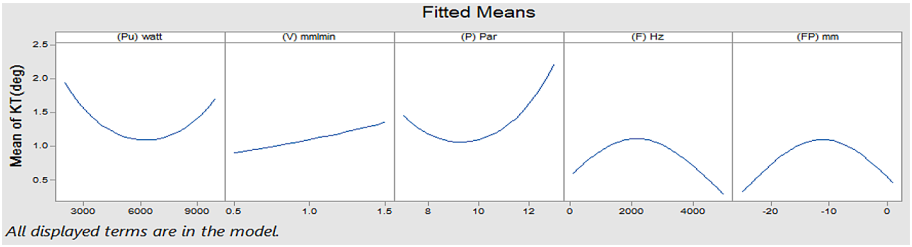

Figure 14. Main effects plot influence of machining parameters on the KT

trend – moderate pressure minimized KT, while low or high levels increased it. Pulse frequency also showed a nonlinear effect, with KT lowest at mid-range values. Cutting speed caused a steady increase in KT. In contrast, laser power and focal position had minimal influence. These results align with the contribution percentages, confirming P, F, and v as key variables to control KT.

Interaction effects and physical interpretation

Figures 15, 16, and 17 collectively illustrate the interaction effects of machining parameters TKW, BKW, and KT. A consistent observation across all three plots is the strong interaction between P and both v and FP, suggesting that the effectiveness of P is highly dependent on these two

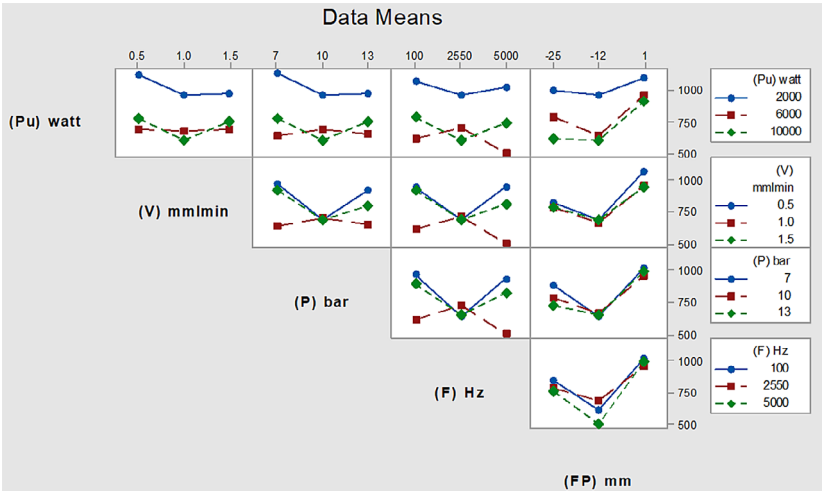

Figure 15. Interaction plot showing the effects of machining parameters on TKW

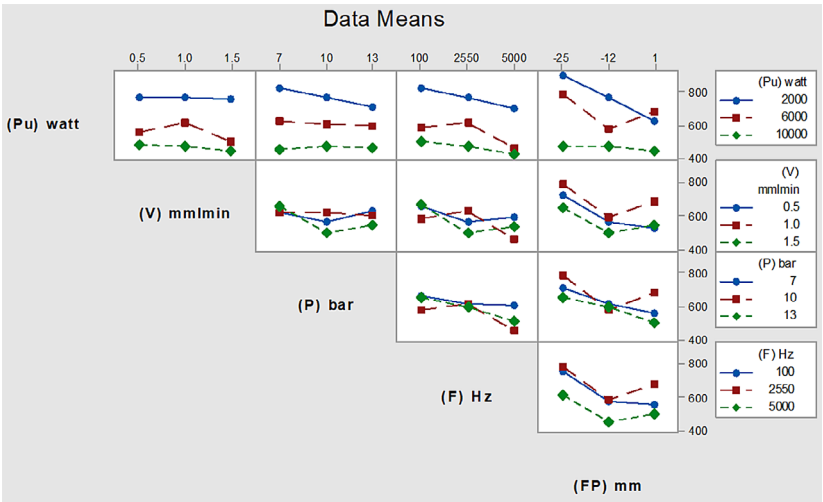

Figure 16. Interaction plot showing the effects of machining parameters on BKW

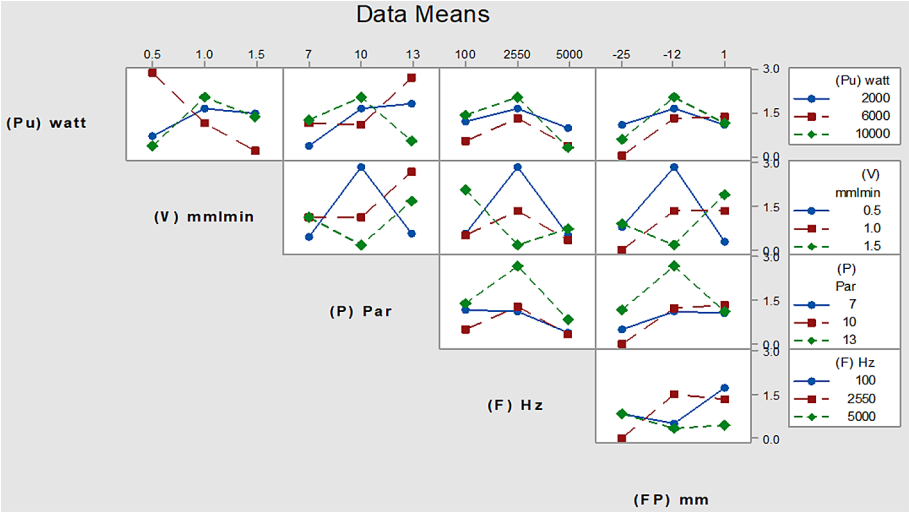

Figure 17. Interaction plot showing the effects of machining parameters on KT

parameters. For instance, the influence of P on KT becomes more pronounced at lower feed rates, likely due to enhanced thermal input and altered gas dynamics, which affect KW and taper formation. Similarly, the interaction between F and FP affects KT through changes in energy distribution, influencing the uniformity of the cut along the material thickness. In contrast, Pu demonstrates a strong individual effect, particularly on BKW (72%) and to a lesser extent on TKW (61%), indicating its significant role in heat accumulation and molten material evacuation. However, its interaction with other parameters is limited, as shown by the nearly parallel trend lines. These findings highlight the need for integrated optimization of parameters, particularly focusing on the interplay between P, v, and FP, to achieve consistent kerf geometry and efficient taper control in laser cutting operations Additionally, the ANOVA results showed that most two-factor interaction terms (e.g., A×B, A×C) were statistically insignificant ($p > 0.05$), indicating weak combined effects. This is likely due to the limited number of experimental runs relative to the number of interaction terms assessed. Future studies should consider expanding the experimental design or using advanced modeling techniques such as machine learning to better capture and interpret these complex interactions.

CONCLUSIONS

This study presented an investigation of how the TKW, BKW, and KT in 201 stainless steel were affected by a number of fiber LC process parameters, including assist gas pressure, frequency, laser power, cutting speed, and focal position. The study's main conclusions are as follows:

- Top kerf width (TKW): Significantly influenced by laser power (61% contribution) and focal position (28%). The minimum TKW achieved was 369.64 µm. These two parameters were critical in controlling the beam width and energy density at the cutting zone.
- Bottom kerf width (BKW): Most affected by laser power (72%), followed by focal position (17%). The lowest BKW obtained was 507.12 µm, highlighting the importance of thermal penetration control.
- Kerf taper (KT): Primarily governed by assist gas pressure (40.6%), frequency (26%), and cutting speed (23%). The optimal KT was minimized to 0.011°.
- The regression model for KT showed low R^2(adj) and R^2(pred), indicating poor prediction capability. This suggests the need for nonlinear or machine learning models in future research
- Achieving optimal kerf quality and taper control requires the joint tuning of gas pressure, cutting speed, and focal position, as these parameters show strong interactions, while laser power has a mainly independent effect, particularly on bottom kerf width.
- It should be noted that while the CCD design provided sufficient resolution for evaluating main effects, the limited number of experimental runs (32) may not be adequate to fully capture higher-order or complex interaction effects among the five input parameters.

Future studies should consider expanding the experimental design or adopting more advanced modeling methods to improve the representation of these multi-factor interactions.

- Although the statistical analysis revealed that individual factors such as laser power (Pu) and gas pressure (P) have the most significant impact on cutting quality, certain two-factor interactions (such as Pu × P or v × F) may indirectly influence the final responses. This indicates the need for future studies to focus on these complex interactions in order to develop more accurate predictive models.
- The results indicated the existence of relatively stable zones at certain parameter levels, such as medium gas pressure or moderate pulse frequency, which yielded improved outcomes in terms of TKW and KT. This suggests the potential to develop a "safe operating window" to ensure consistent cutting quality regardless of minor fluctuations in system conditions.

REFRENCES

1. Dutta, S.K. Different types and new applications of stainless steel, Stainl. steel, 2018; 62(5): 86–91, [Online]. Available: https://www.researchgate.net/publication/330383386
2. Abdullah, M.A., Abed, A.H., Mansor, K.K. Comparison between low-carbon steel and galvanized steel by deep drawing under the influence of different parameters. Management Systems in Production Engineering, 2025; 33(2): 163–170.
3. Gujarati, D. and Porter, D. Performance evaluation of nitrogen gas-assisted laser cutting on 316l austenitic stainless steel plate, no. May, 2010.
4. Genna, S., Menna, E., Rubino, G. and Tagliaferri, V. Experimental investigation of industrial laser cutting: The effect of the material selection and the process parameters on the kerf quality, Appl. Sci., 2020; 10(14), https://doi.org/10.3390/app 10144956
5. Kotadiya, D.J., Kapopara, J.M., Patel, A.R., Dalwadi, C.G. and Pandya, D.H. Parametric analysis of process parameter for Laser cutting process on SS-304, Mater. Today Proc., 2018; 5(2): 5384–5390, https://doi.org/10.1016/j.matpr. 2017.12.124
6. Syarifah, "investigation of laser cutting parameters on surface quality of stainless steel," Africa Educ. Rev., 2010; 15(1): 156–179, [Online]. Available, http://epa.sagepub.com/content/15/2/129.short%0Ahttp: //joi.jlc.jst.go.jp/JST. Journalarchive/materia1994/46.171?from=CrossRef
7. Zabon, A.H., Abbas, T.F., Bedan, A.S. Enhancing laser cutting quality of stainless steel 201 by controlling dross formation and surface roughness using multi-factor experimental design, Advances in Science and Technology Research Journal, 2025; 19(7): 458–470.
8. Orishich, A.M., Malikov, A.G., Shulyatyev, V.B. and Golyshev, A.A. Experimental comparison of laser cutting of steel with fiber and CO_2 lasers on the basis of minimal roughness, Phys. Procedia, 2014; 56(C): 875–884, https://doi.org/10.1016/j.phpro.2014.08.106
9. Pramanik, D., Kuar, A.S., Sarkar, S. and Mitra, S. Enhancement of sawing strategy of multiple surface quality characteristics in low power fiber laser micro cutting process on titanium alloy sheet, Opt. Laser Technol., 2020; 122(September 2019): 105847, https://doi.org/10.1016/j.optlastec.2019.105847
10. Patel, A. and Bhavsar, S.N. Experimental investigation to optimize laser cutting process parameters for difficult to cut die alloy steel using response surface methodology, Mater. Today Proc., 2020; 43: 28–35, https://doi.org/10.1016/j.matpr.2020.11.201
11. Rajamani, D., Siva Kumar, M., Balasubramanian, E. and Tamilarasan, A. Nd: YAG laser cutting of Hastelloy C276: ANFIS modeling and optimization through WOA, Mater. Manuf. Process., 2021; 36(15): 1746–1760, https://doi.org/10.1080/10426914.2021.1942910
12. Alsaadawy, M., Dewidar, M., Said, A., Maher, I. and Shehabeldeen,T.A. Investigation of the effect of laser cutting parameters on surface and kerf quality of thick Ti–6Al–4V alloy sheets, Arab. J. Sci. Eng., 2024, https://doi.org/10.1007/s13369-024-09083-6
13. Li, M., Chen, L. and Yang, X. A feasibility study on high-power fiber laser cutting of thick CFRP laminates using single-pass strategy, Opt. Laser Technol., 2021; 138(December 2020): 106889, https://doi.org/10.1016/j.optlastec.2020.106889
14. Singh, Y., Singh, J., Sharma, S., Aggarwal, V. and Pruncu, C.I. Multi-objective optimization of kerf-taper and surface-roughness quality characteristics for cutting-operation on coir and carbon fibre reinforced epoxy hybrid polymeric composites during CO_2-pulsed laser-cutting using RSM, Lasers Manuf. Mater. Process., 2021; 8(2): 157–182, https://doi.org/10.1007/s40516-021-00142-6
15. Nguyen, V., Altarazi, F. and Tran, T. Optimization of process parameters for laser cutting process of stainless steel 304: A comparative analysis and estimation with taguchi method and response surface methodology, Math. Probl. Eng., 2022; 2022, https://doi.org/10.1155/2022/6677586
16. Patidar, D. and Rana, R.S. The effect of CO_2 laser cutting parameter on Mechanical & Microstructural characteristics of high strength steel-a review, Mater. Today Proc., 2018; 5(9): 17753–17762, https://

doi.org/10.1016/j.matpr.2018.06.099

17. Pacher, M., Franceschetti, L., Strada, S.C., Tanelli, M., Savaresi, S.M. and Previtali, B. Real-time continuous estimation of dross attachment in the laser cutting process based on process emission images, J. Laser Appl., 2020; 32(4), https://doi.org/10.2351/7.0000145
18. Mansor, K.K., Shabeeb, A.H., Hussein, E.A., Abbas, T.F., Bedan, A.S. A statistical investigation and prediction of the effect of FDM variables on flexural stress of PLA prints, J. Tikrit of engineering sciences 2024; 31(3): 10–17.
19. Ghazi, S.K., Salloom, M.Y., Bedan, A.S. Experimental evaluation of a system to control the incremental forming of aluminum alloy type 1050, Engineering Technology and Applied Science Research, 2024; 14(5):16943–16949.
20. Rakesh Ch., Vora, J.J., Patel, V., de Lacalle L.N.N. and Parikh, D.M. Surface analysis of wire-electrical-discharge-, MDPi, 2020; 2: 6–9.
21. Bedan, A.S., Shabeeb, A.H., Hussein, E.A. Improve single point incremental forming process performance using primary stretching forming process, Advances in Science and Technology Research Journal, 2023; 17(5): 260–268.
22. Oğuzhan, D.E.R., Gökhan, B.A.Ş.A.R., Muhammed, O.R.D.U. Statistical investigation of the effect of CO_2 laser cutting parameters on kerf width and heat affected zone in thermoplastic materials, JournalMM, 2023; 4(2): 459–474.